Direct Nanoimprinting of a Colloidal Self-Organizing Nanowire Ink for Flexible, Transparent Electrodes

Johannes H. M. Maurer, Lola González-García, Indra K. Backes, Beate Reiser, Sarah M. Schlossberg, and Tobias Kraus**

A semicontinuous process is used to nanoimprint a nanowire ink and form transparent conductive electrodes. Ultrathin gold nanowires are confined in the features of an elastomeric stamp, where they spontaneously assemble upon drying into hierarchical, percolating superstructures. This templated self-organization yields grids with defined line widths down to 0.9 µm and high pattern fidelity. Metal grids with square, hexagonal, and linear features are printed over 30 cm^2 on different substrates and gently sintered in hydrogen plasma. Meshes on polyethylene terephthalate foil show high optical transmittances (>92%) and low sheet resistances (106–168 Ω sq^{-1}). Their resistance is changed by only 10% after 500 bending cycles at a radius of 5 mm. The printed electrodes are used to build capacitive and resistive touch sensor devices.

1. Introduction

Printing electronic devices from "inks" that contain dispersed nanostructures provides several potential benefits. Additive deposition of electronic materials from liquid dispersion reduces the required amount of material.[1] Printing at room temperature is inherently compatible with many substrates, for example polymer films that are used for flexible displays[2] or integrated sensors.[3] Inks for printed electronics have been prepared using dissolved or dispersed conductive polymers and colloidal dispersions of inorganic nanoparticles. Polymer inks are easy to use but provide only limited conductivity and tend to degrade by oxidation.[4] Metal nanoparticles are suitable to print highly conductive traces and electrodes; synthetic protocols are readily available for such particles, and the inherent conductivity of metals is large.[5] Inks based on metal nanoparticles have been structured on substrates using screen-,[6] gravure[7] or inkjet-printing,[8] laser sintering,[9,10] flow coating,[11] and evaporative lithography,[12,13] among others. Each printing technique has specific advantages and disadvantages, but two limitations are very common: (1) resolution is limited to several micrometers; (2) sintering at increased temperatures is required to remove the organic ligands that stabilize the nanoparticles in dispersion, which limits the choice of suitable substrate materials. Emerging concepts to overcome this limitation include "sintering-free" inks[14] and alternative sintering approaches at low temperatures.[15]

Transparent flexible electronics demand both high resolution of the printed patterns and low thermal impact. Printed metal grids on polymer foils are a promising alternative to the incumbent for rigid substrates, ITO (indium tin oxide), which is brittle and requires high-temperature processing.[16,17] High optical transparency and high electrical conductivity can be achieved using thin metal lines that provide electrical conduction and are separated by voids that transmit optically. Line width and pitch of the grid determine transparency and conductivity and have to be adjusted according to the desired properties. An increased line width will decrease transparency and resistance, an increased pitch will cause the opposite.[18,19] Conventional printing techniques have minimum feature sizes of several micrometers, which implies a large pitch to achieve sufficient transparency. Metal lines with several micrometer widths tend to be visible depending on illumination and limit the grids' applicability as front electrode of displays, for example.

Established printing processes for electronics are based on the "active" structuring of a "passive" ink. The ink is optimized to follow the structures imposed by the printing process. We recently introduced an ink that takes a more active part: dispersed nanowires self-organize into hierarchical superstructures during imprinting and guarantee the formation of a percolating mesh.[20] The wires have an aspect ratio exceeding 1000 and are flexible enough to follow microscale features of an elastomeric stamp. Supramolecular interactions between the ligand molecules induce bundling when the wires reach a certain concentration inside the stamp.[21] The geometry of the structuring template is faithfully reproduced and supplemented by a structure that depends on the wires' interactions. Line contacts between the wires induce the formation of well-defined bundles of parallel wires that accumulate all metal content; the wires' concentration ultimately sets the width of lines formed inside the stamp.[20,21] The wires interdigitate inside the bundles like wool fibers in a yarn, ensuring percolation over macroscopic distances even at relatively low ink concentrations. Thus, the ink "actively" takes part in the patterning process and is a key to achieve high resolution.

J. H. M. Maurer, Dr. L. González-García, I. K. Backes, B. Reiser, S. M. Schlossberg,[+] Prof. T. Kraus
INM—Leibniz Institute for New Materials
Campus D2 2, 66123 Saarbrücken, Germany
E-mail: lola.gonzalez-garcia@leibniz-inm.de; tobias.kraus@leibniz-inm.de

[+]Present address: Department of Nanoengineering, University of California, San Diego, 9500 Gilman Drive, La Jolla, CA 92092, USA

DOI: 10.1002/admt.201700034

In this paper, we demonstrate the imprinting of a self-organizing ink in a semicontinuous process. The self-organization process is analyzed by gracing incidence small-angle X-ray scattering. Grids of squares, hexagons, and lines were printed on polymer foils, glass, and paper over areas of up to 30 cm^2 and analyzed for electrical and optical properties. Square grids were tested as transparent and flexible electrodes in touch sensors.

2. Results and Discussion

2.1. Printing Process and Setup

Figure 1a shows a schematic illustration of the semicontinuous imprinting process: a prepatterned elastomeric stamp (1) is attached to a roller. As the roller moves on a substrate, the nanowire ink (2) is confined into the cavities of the stamp. The nanowires are sufficiently flexible to follow grooves in the stamp as a low-viscosity ink. The solvent diffuses through the stamp and the ink dries while the stamp is in contact (3). Upon drying, the wires self-assemble into hierarchical bundles that pervade the stamp's connected grooves (4). The roller speed has to be adjusted to balance solvent transport and imprinting: the forming mesh must be sufficiently dry before the stamp is peeled off to avoid deterioration of the lines. Conventional nanoimprinting usually aims at precisely replication of the stamp's features in the material. The process introduced here uses lower solid contents; it forms lines in the center of the stamp's grooves that are much smaller than the grooves and easily detach from the stamp.

Figure 1b shows a photograph of a prepatterned polydimethylsiloxane (PDMS) stamp carrying a hexagonal pillar array with a pitch of 19.5 µm and a pillar spacing of 1.8 µm. A homogeneous thickness of the stamp is crucial to reach an equal pressure distribution and conformal contact to the substrate. The prepatterned PDMS stamp was attached on a steel roller, which was then mounted on a tool carrier of a commercial film applicator that controls the speed of the forward movement (Figure 1c, a video of the imprinting process can be found in Movie S1 of the Supporting Information). The applied pressure was determined by the weight of the roller and was adjusted using different rollers to achieve a homogeneous filling of the cavities and an effective ink-removal between pillar and substrate. Higher pressure caused deformation and collapsing of the PDMS pillars that lead to incomplete filling of the cavities and decreased pattern fidelity of the printed grid. Lower pressure led to residual layers outside the desired pattern where the stamp did not fully displace the liquid.[22]

The cylindrical stamp configuration has several advantages over a flat conformal contact. The reduced contact area between substrate and stamp decreases the force that is required.[23] The effective ink-stamp contact area is decreased, which leads to a lower concentration of the diffusing solvent in the bulk of the stamp that decreases swelling and improved fidelity. The semicontinuous rolling geometry is a first step toward future implementation in a continuous roll-to-roll process.

2.2. Self-Organizing Ink

The inks used here were based on ultrathin gold nanowires (AuNWs) with diameters around 1.6 nm and aspect ratios above 1000 prepared in a scalable synthesis that forms wires that are capped by an oleylamine (OAm) ligand layer.[24] Their small diameter lends them mechanical flexibility and mobility

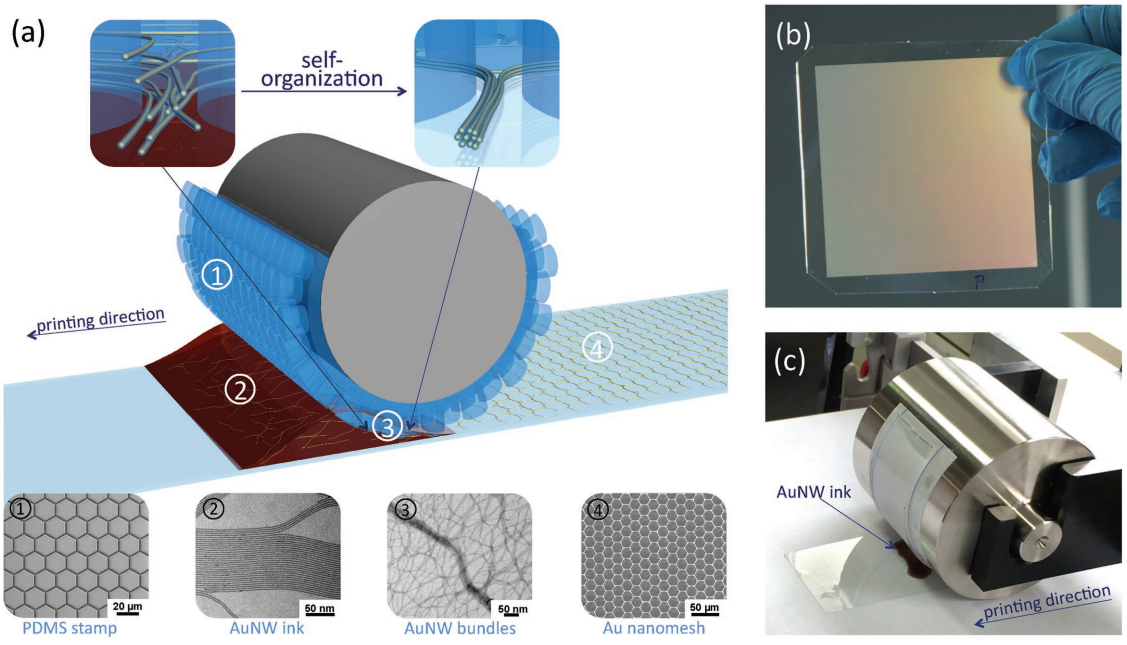

Figure 1. a) Schematic illustration of the imprinting process (1: SEM image of a PDMS stamp with hexagonal pillar array; 2: TEM image of as-synthesized ultrathin gold nanowires; 3: TEM image of a gold nanowire bundle; 4: SEM image of a printed hexagonal metal grid on PET). b) Photograph of a PDMS stamp carrying hexagonal pillar arrays. c) Photograph of the imprinting setup.

in dispersion. Both mobility and flexibility are required for the complete filling of the stamp's cavities. The flexibility eases wire–wire contact and the formation of multivalent bonds between the OAm ligand molecules of adjacent wires, which leads to self-organization into hierarchical bundles of wires.[21,25,26] The wires in each line of the stamp have to accumulate in a single thread to electrically connect macroscopic areas after annealing. Self-organization achieves this by forming a compact fiber from the AuNWs that percolate throughout the electrode pattern even at low metal concentrations down to 2 mg mL^{-1} (i.e., 0.13 vol% solid content).

It is critical that the self-organization of the wires occurs at an appropriate stage of the process: bundling should not occur already in dispersion, but only when the solvent evaporates. The high mobility of the single wires is thus preserved during the imprinting process so that the wires uniformly distribute in the cavities. The onset of the bundling is a function of the used solvent. Cyclohexane keeps single wires dispersed at the ink concentration and was therefore used for the imprinting process.[21]

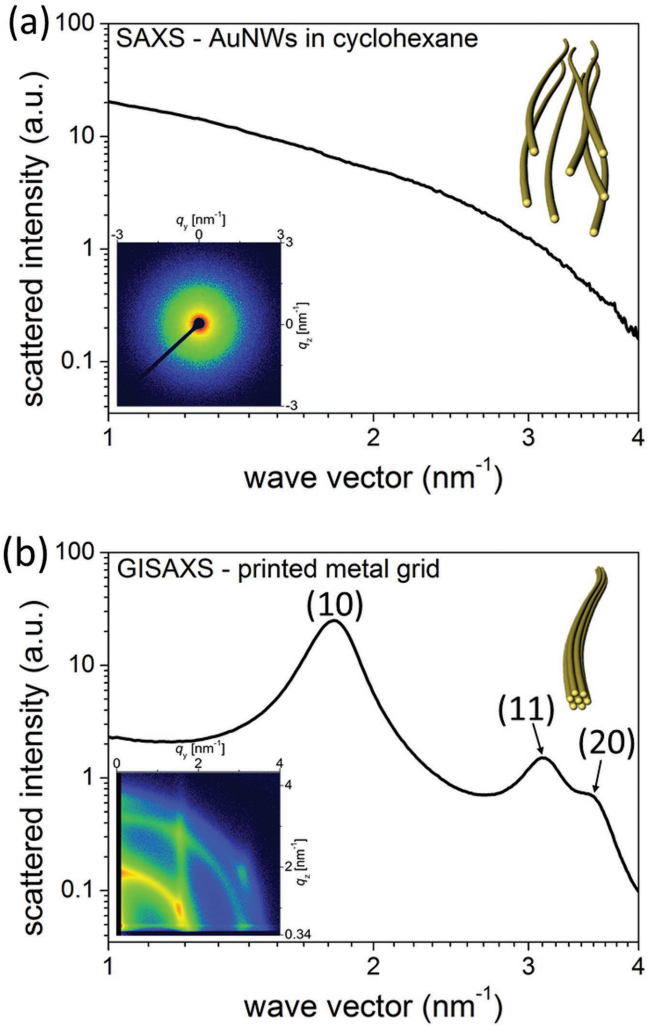

Figure 2. a) SAXS pattern of AuNWs dispersed in cyclohexane. Inset: corresponding 2D pattern. b) GISAXS pattern of a printed metal grid with linear geometry on glass before plasma treatment. Inset: corresponding 2D pattern.

Figure 2a shows a small-angle X-ray scattering (SAXS) pattern of gold nanowires dispersed in cyclohexane (concentration: 4 mg mL^{-1}). The pattern shows no peaks of structural ordering, which confirms the unbundled state of the wires in dispersion. The concentration of the ink tunes the line widths of the grid and can be varied in a wide range without agglomeration of the wires (up to at least 15 mg mL^{-1}). In the experiments discussed here, AuNW content was varied between 2 and 8 mg mL^{-1} to tune the feature size in the desired range (see below). The viscosity of the ink was very close to that of the neat solvent.

The arrangement of the wires in the printed metal grids was studied by gracing incidence small-angle X-ray scattering (GISAXS). The experimental setup is shown as Figure S1 in the Supporting Information. Figure 2b shows the scattering of a printed metal grid with linear geometry on glass (before plasma treatment, lines oriented parallel to incoming beam). The inset shows the corresponding 2D pattern. Distinct Bragg peaks appear; the relative spacing of the first peaks indicates hexagonal ordering (1:$\sqrt{(3:2)}$).[27,28] The results are in line with recent studies on the hexagonal arrangement of AuNWs inside bundles formed in dispersion.[21,25] The evolution of the long-range order peaks underlines the controlled organization process and a dense packing of parallel wires in the superstructures.

Self-organized wires are not electrically conductive, because the organic OAm shell that is required in AuNW synthesis and aids self-organization constitutes a tunnel barrier for electrons. A "soft" plasma sintering step in a hydrogen/argon plasma removed the insulating ligand shell and coarsened the structure to improve stability.[29,30] The sintering step was performed at room temperature and is compatible to a variety of substrates. We followed the structural effects of plasma sintering in the GISAXS patterns: single-wire peaks disappeared as the wires sintered into larger superstructures revealing the complete sintering of the wire bundles (see Figure S2, Supporting Information).[29]

2.3. Geometry, Conductivity, and Transparency of Metal Grids Printed on Polyethylene Terephthalate (PET) Foil

Figure 3 shows scanning electron micrographs of printed metal grids with square, hexagonal, and linear geometry on a PET foil after plasma treatment. The images reveal a high fidelity of the patterns. All grids were printed using PDMS stamps with a pitch of 19.5 µm, a pillar spacing of 1.8 µm, and a pillar height of 4 µm. Electron micrographs of the corresponding stamps can be found in Figure S3 of the Supporting Information. All meshes were printed at a speed of 5 mm s^{-1} and a nanowire concentration of 4 mg mL^{-1}. Other mesh geometries are readily accessible using appropriate stamps.

Table 1 summarizes dimensions, electrical conductivities, and optical transmittances of the different grids. The dimensions of the grids were characterized by atomic force microscopy (AFM) (see also Figure S4, Supporting Information). The average line widths depended on the overall geometry even for identical pitches and AuNW concentrations: linear grids had the largest widths (w = 1.7 µm), followed by square (w = 1.41 µm) and hexagonal (w = 1.39 µm) geometries. All square meshes (and only they) exhibited anisotropies that

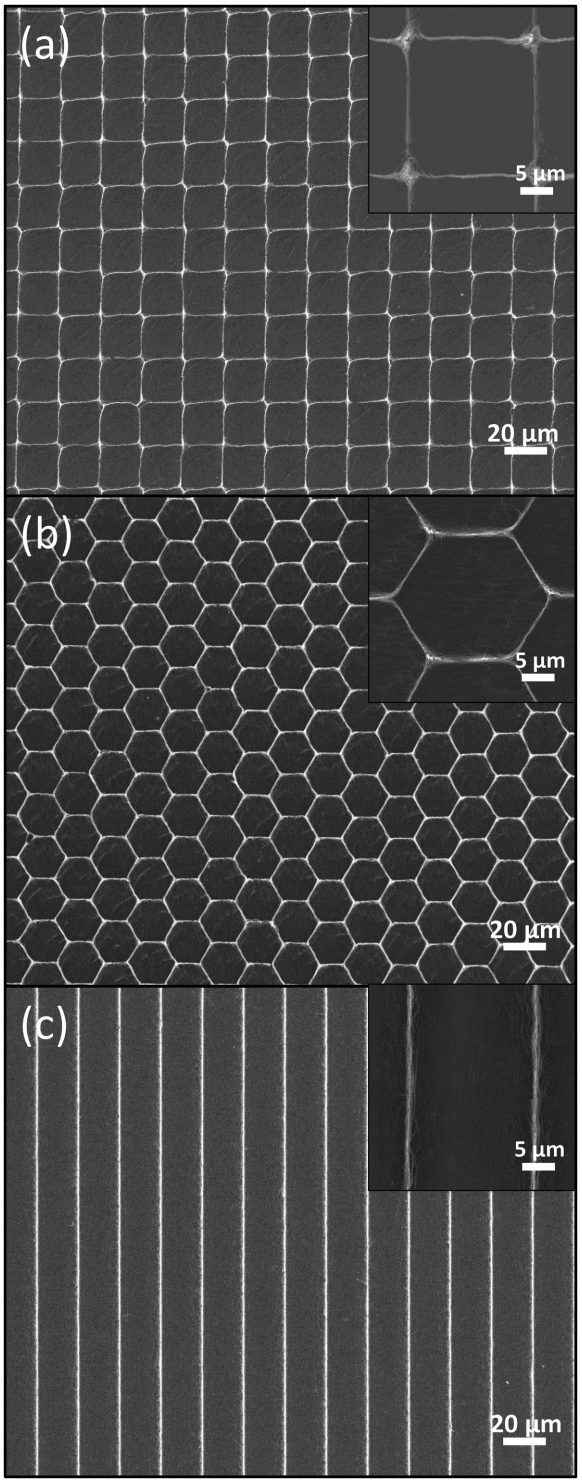

Figure 3. SEM images of printed metal grids on PET (AuNW concentration: 4 mg mL^{-1}; printing speed: 5 mm s^{-1}) with a) square, b) hexagonal, and c) linear geometry after plasma treatment. Insets show magnified printed lines after sintering.

depended on the printing direction. Lines perpendicular to the printing direction were narrower and higher (average width w = 0.91 µm and height h = 70 nm) than those parallel to the printing direction (average width w = 1.41 µm and height h = 60 nm). Such differences can be explained by the dynamics of the imprinting process: mesh geometry and quality are strongly influenced by the convection of ink inside the stamp's cavities and the permeation of solvent through the stamp; both strongly depend on stamp geometry. Square and hexagonal grids enable cross-flow between the channels, while ink in the linear can only flow parallel to the printing direction. The stamp geometry also affects the deformation of the pillars under compression by the cylinder. Stamps with different geometries thus lead to different mesh dimensions and structural defects at the same ink concentration, pillar spacing, and printing parameters.

Table 1. Geometrical, optical, and electrical properties of the printed metal grids on PET.

Geometry	Line width [µm]	Maximal line height [nm]	R_{sheet} [Ω sq^{-1}]	Transmittance @ 500 nm [%]
Squares[a)]	1.41 ± 0.21	60 ± 5	128 ± 13	92.3 ± 0.5
Squares[b)]	0.91 ± 0.12	70 ± 7	196 ± 36	
Hexagons	1.39 ± 0.15	76 ± 5	168 ± 12	93.3 ± 0.3
Lines	1.70 ± 0.26	66 ± 6	106 ± 12	93.4 ± 0.4

[a)]Parallel to printing direction; [b)]Perpendicular to printing direction.

Structural differences between grids are reflected in their electrical and optical properties. Linear meshes had the lowest sheet resistances (measured along the lines), followed by hexagonal and squares meshes. The anisotropy of the square meshes discussed above led to anisotropic electrical properties (see Table 1): the sheet resistance measured parallel to the printing direction was smaller (R_{sheet} = 128 Ω sq^{-1}) than that measured perpendicular to it (R_{sheet} = 196 Ω sq^{-1}). It is useful to compare the measurements to theoretical resistances calculated using Kirchhoff's rules for a perfect grid with the bulk resistivity of gold as described in the Supporting Information. The measured resistances were ≈13–24 times above the theoretical limits, similar to previous reports on nanoparticle-based electrodes that attributed such differences to grain boundary scattering, nanopores, variations of the line width, and structural grid defects.[20,31] Figure S5 (Supporting Information) shows a high resolution Scanning Electron Microscopy (SEM) image of a printed line after plasma sintering. Hexagonal meshes are likely to have lower conductivities due to a larger amount of grid defects (see Figure S6, Supporting Information).

All meshes exhibited optical transmittances >92% over the entire visible range. **Figure 4** shows representative optical ballistic transmittance spectra of the printed metal grids on PET for the different mesh geometries. The meshes used in this work were designed for transparent touch sensors, where high optical transmittance has priority over high conductivity.

We successfully printed metal grids on glass, paper, and cling wrap, too. Results on paper and glass can be found in Figures S7 and S8 in the Supporting Information. Optical microscopy confirmed uniformity over large areas for glass (see Figure S9, Supporting Information). Adjusting the AuNW concentration changed the line width and height and allowed us to

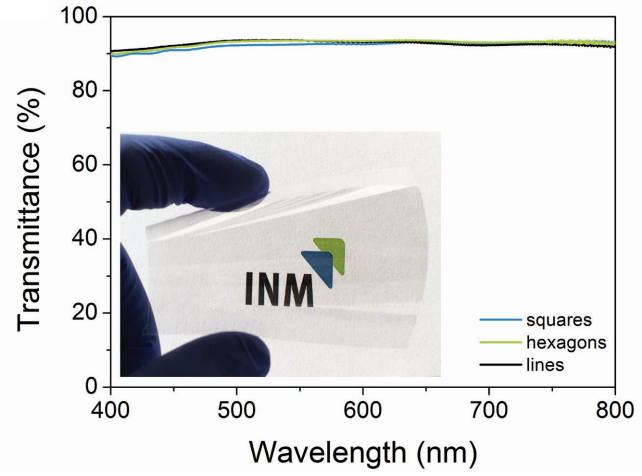

Figure 4. Representative optical ballistic transmittance spectra of the different printed metal grids. Inset shows a photograph of a printed square mesh on PET.

tune the transparency/conductivity ratio as shown in Figure S8 (Supporting Information).

2.4. Mechanical Properties of Printed Metal Grids on Flexible Substrates

Metal-based grid electrodes are mechanically flexible. **Figure 5**a shows the mean variation in sheet resistance ($(R - R_0)/R_0$) of square, hexagonal, and linear grids printed on PET during cyclical bending at a radius of 5 mm under tension. The sheet resistance of a commercial ITO-coated PET foil (Sigma-Aldrich, $R_0 = 100\ \Omega\ sq^{-1}$) increased by more than 2 orders of magnitude after 50 cycles. The resistance of printed square and hexagonal meshes showed asymptotic behavior with an increase of 5%–7% during the first 50 bending cycles and only 10% increase after 450 additional cycles. Linear grids increased resistance along the lines by 10% after 500 cycles when bending parallel (0°) to the line direction and 30% when bending perpendicular (90°). We believe that crack formation that leads to grid defects and reduced connectivity of the mesh is the predominant mechanism. Linear grids are severely affected by a single crack in a conductive line and particularly sensitive to deformation, while square and hexagonal meshes only loose small parts of the interconnected network after such a crack.

Photographs in Figure 5b,c show a square metal grid printed on PET with two commercial light-emitting diodes (LEDs) mounted in the center. Bending and twisting of the mesh did not visibly change the emission of the LEDs. We also tested a soft substrate that causes larger deformations of the wires than PET foil. A square metal grid was printed on a 10 µm thick polyethylene foil ("cling wrap," Figure 5d, left). The thin foil is very flexible and sticky. The sheet resistance of the printed grid was increased to ≈1 $k\Omega\ sq^{-1}$, probably due to dense structural defects in the grid on the soft substrate. The layer retained a conductivity on its original order of magnitude after crushing, unfolding, and furling along a cannula (diameter: 1.1 mm) (see also Figure S10, Supporting Information).

2.5. Application

Capacitive and resistive touch devices are important applications of transparent conductive materials. We tested the applicability of our meshes for such devices. **Figure 6**a shows a transparent capacitive touch sensor based on a square metal grid on a PET foil ($5 \times 6\ cm^2$) that was subdivided into four different segments. Touching the backside of the coated PET foil reliably caused a change in capacitance that was detected by a

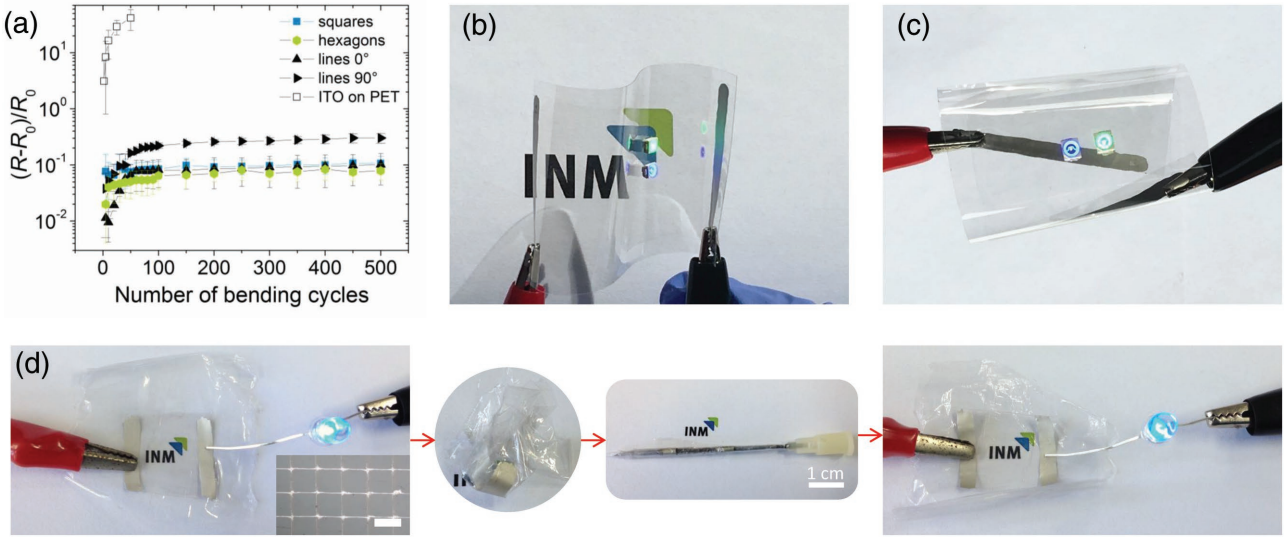

Figure 5. a) Averaged normalized change in resistance $(R - R_0)/R_0$ as a function of bending cycles under tension for the printed gold metal grids and a commercial ITO film on PET. b) The bending radius was 5 mm. c) Photographs of a square metal grid on PET with two LEDs upon bending and twisting. d) Photographs of a square metal grid printed on cling wrap. Inset: optical microcopy image of the printed mesh. Scale bar: 10 µm. The layer remained conductive even after crushing and unfolding and subsequent folding around a cannula.

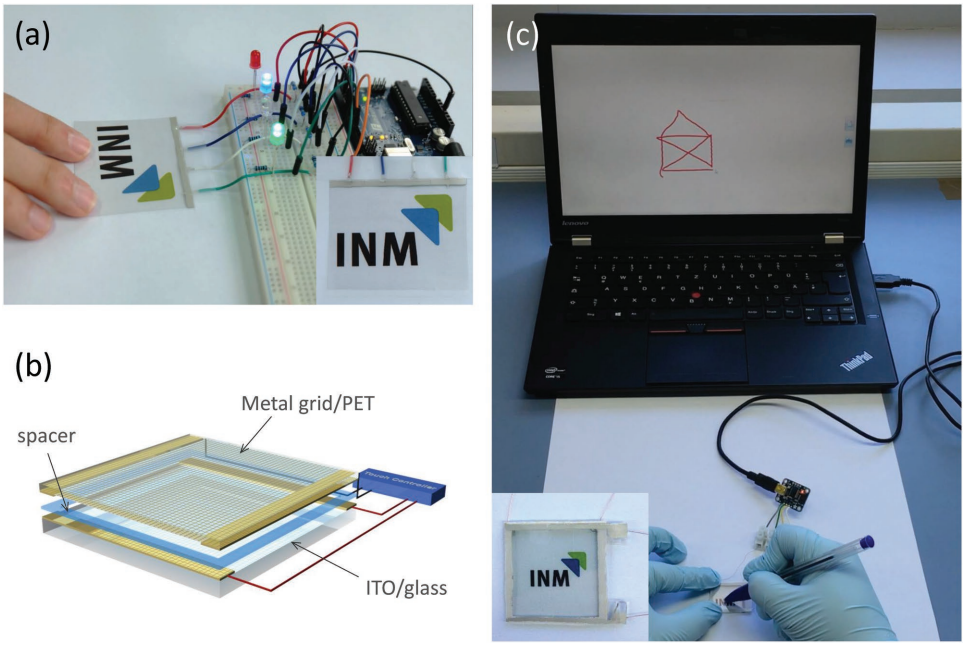

Figure 6. a) Photograph of the capacitive touch sensor operation. Upon touching the backside of the coated PET foil, LEDs could be switched on and off with a microcontroller. b) Schematic diagram of the resistive touch sensor fabricated using a printed metal grid on PET. c) Photograph of the resistive touch sensor operation.

microcontroller so that LEDs could be switched on and off with fast response. Movie S2 in the Supporting Information shows the dynamics of the capacitive sensor.

A second mesh on PET was used as a resistive touch device. Figure 6b shows a schematic diagram of the setup. The sensor consisted of an ITO-coated glass slide as rigid substrate and a square metal grid on PET as top electrode. The electrodes were mounted on a thin frame of double-sided tape to create a uniform gap and align the conductive surfaces. When pressing the coated PET foil down, the two electrodes came into contact and acted as a voltage divider at the point of contact. The point of contact was determined by measuring the voltage change through a commercial touch controller. Figure 6c shows a photograph of the resistive touch device in operation. We drew the "House of Nikolaus" (Eulerian path); a video of the touchscreen in operation is included in Movie S3 of the Supporting Information.

3. Conclusion

Metal grids composed of uniform lines were printed by direct nanoimprinting of a self-organizing ink at ambient conditions. Ligand-controlled supramolecular interactions between ultrathin gold nanowires provoked bundling of the wires into hierarchical superstructures that followed the geometry of an elastomeric stamp. The mesh structure was predefined by the stamp geometry, but the dimensions of the connecting lines were determined by the self-organization of the ink. Percolation stemmed from the bundling of wires with large aspect ratios. A semicontinuous process was used to print large arrays (up to 30 cm^2) on PET, glass, paper, and cling wrap. Metal grids with different geometries (squares, hexagons, lines) on PET foils exhibited high optical transmittances of >92% at 500 nm and sheet resistances in the range of 106–168 Ω sq^{-1}. The meshes could be bent without losing conductivity even after hundreds of cycles. We showed that capacitive and resistive transparent touch sensors can be readily built using our methods and suggest that transparent sensors integrated in furniture or windows are possible using our meshes on adhesive foils. Other fields of application include multielectrode arrays for biomedical or implantable electronics that profit from the inertness of gold and the mechanical flexibility that the meshes provide. We are convinced that the process can be scaled to roll-to-roll setups for the production of square meter areas.

The combination of nanoimprinting and self-organization that underlies this process is a promising concept that is not limited to the presented material system. Other inks with interacting particles that exhibit controlled agglomeration in polymer-particle composites and semiconductor particle films are currently investigated. More complex stamps can be used to create meshes with multiple levels of hierarchy.

4. Experimental Section

Ink Preparation: Ultrathin gold nanowires were synthesized as described in previous works.[20,24] In a typical synthesis, 100 mg of $HAuCl_4 \times 3H_2O$ were dissolved in a mixture of 4.55 mL oleylamine (technical grade, 70%, Sigma-Aldrich, Germany) and 15.35 mL of *n*-hexane (99%, ABCR, Germany). An amount of 6.55 mL of triisopropylsilane (98%, ABCR, Germany) was added to the solution and the reaction was kept undisturbed at RT overnight. The wires were precipitated by adding 70 mL of a mixture of ethanol/methanol (95/5, v/v). The supernatant was removed and the wires were redispersed in n-hexane. The washing step was repeated once and the wires were finally redispersed in cyclohexane to the desired concentration.

Fabrication of PDMS Stamps: The PDMS stamps were prepared in a two-step molding process using a lithographically fabricated silicon

master (AMO GmbH, Germany) that carried the desired pattern (patterned area: 7 × 7 cm^2) of the final stamp. A PDMS replica of the silicon master acted as a mold in the final stamp fabrication. The molding procedure was identical for both steps: the prepolymer and the cross-linker of a PDMS kit (Sylgard 184, Dow Corning) were mixed in a 10:1 weight ratio and degassed in a Speedmixer 5000 HP (Hauschild & Co KG, Germany) at a speed of 2350 rpm and a pressure of 1 mbar for 3 min. The mixture was then poured on the structured mold (silicon or PDMS), which had been silanized with a trichloro(octadecyl)silane (Sigma-Aldrich, Germany) before. Homogeneous thickness of the PDMS layer was ensured by a Teflon ring that acted as spacer and a glass plate as top sealing. The PDMS was then fully cured at 70 °C overnight. After that, the PDMS replica was peeled off. We used stamps that carried a square, hexagonal, or line array with a pitch of 19.5 µm, a spacing of 1.8 µm, and a height of 4 µm.

Semicontinuous Nanoimprinting Setup: The PDMS stamp was attached to a steel roller with a diameter of 8 cm and a weight of 6 kg (pressure ≈1.4 bar) using double-sided tape. The roller was then mounted on the tool carrier of a commercial film applicator (TQC GmbH, Germany) with a home-built holder. The linear movement of the carrier was translated into a rolling motion of the steel roller with the attached stamp.

Substrate Materials: Glass (microscope slide; Paul Marienfeld, Germany); PET foil (Melinex 400; DuPontTeijinFilms, Luxembourg); paper (p_e:smart; Felix Schoeller Group, Germany); cling wrap (Aldi Sued, Germany).

Nanoimprinting Process: A volume of 2 µL AuNW dispersion in cyclohexane per cm^2 stamp size was dispensed onto the respective substrate. Cling wrap was stretched and mounted on a glass substrate prior to printing. The imprint procedure was immediately started (see Movie S1, Supporting Information). Its speed was varied in a range between 5 and 6 mm s^{-1}. After imprinting, layers were carefully rinsed with ethanol (≥99.8%, Sigma-Aldrich) to remove excess oleylamine and dried under nitrogen stream. Plasma treatment was performed in a RF PICO plasma system (Diener electronic, Ebhausen, Germany) operating at 0.3 mbar gas pressure and 100 W RF (13.56 MHz) power using mixture of 5% hydrogen in argon for 20 min. Residues on the stamp could be removed by scotch tape or in a potassium iodide solution (1:4:40 I_2:KI:H_2O) before reuse when required.

Capacitive Touch Sensor: In order to individually address different segments, a continuous mesh was electrically subdivided by scratching the layer with the tip of a tweezer. The four different segments were contacted with silver paste and connected to a UNO R3 microcontroller board (Funduino, Germany).

Resistive Touch Sensor: The resistive touch sensor consisted of an ITO-coated glass slide (8–12 Ω sq^{-1}, Sigma-Aldrich) and a square metal grid on PET as top-electrode that were separated by a thin frame of double-sided tape (3M, Germany). Contacts were made by silver paste and the electrodes were connected to a commercial touch screen controller (AR 1100, Adafruit Industries, US) by copper wires. The control software was provided by Adafruit, too.

Characterization: SEM images were acquired using a Quanta 400 ESEM (FEI, Germany). TEM images were recorded using a JEM 2010 (JEOL, Germany) operating at 200 kV. Optical microscopy was carried out using an Eclipse LV100 ND (Nikon Instruments, Netherlands). AFM measurements in tapping mode were recorded using a NanoWizard3 (JPK Instruments, Germany). Optical characterization was conducted by UV–vis spectroscopy in transmission mode (Cary 5000, Varian). The respective substrates were taken as references. SAXS and GISAXS measurements were conducted on a Xeuss 2.0 system (Xenocs SA, France) with a Cu Kα X-ray source (λ = 0.154 nm) operating at 50 kV and 0.6 mA and a Hybrid Photon Counting detector (PILATUS 1M, DECTRIS, Baden, Switzerland). The sample-detector distance was 583 mm. Measurements of the wires in dispersion were performed using capillaries with an inner diameter of 2 mm. The GISAXS pattern was acquired at 0.6° incident angle. The printed lines were oriented parallel to the beam direction. Electrical resistance was measured in a 2-point configuration on an area of 1.5 × 1.5 mm^2 with an ohmmeter (Voltcraft, Germany). Contacts were made with silver paste. To test the change in resistance upon bending, the gold metal grids on PET were bent under tension around a steel rod with a radius of 5 mm; electrical resistance was measured in the flat state.

Supporting Information

Supporting Information is available from the Wiley Online Library or from the author.

Acknowledgements

The authors would like to thank Eduard Arzt for his continuing support of the project, Arzu Colak and Marius Gipperich for the help with the AFM measurements, Manuel Hawner for the help with the stamp fabrication, Sebastian Beck for his help with the imprinting setup, and Marcus Koch for his assistance with the SEM measurements. Funding from the German Federal Ministry of Education and Research in the "NanoMatFutur" program is gratefully acknowledged.

Conflict of Interest

The authors declare no conflict of interest.

Keywords

metal grids, nanoimprinting, self-organization, transparent flexible electrodes, ultrathin gold nanowires

Received: February 7, 2017
Revised: March 2, 2017
Published online: April 20, 2017

[1] A. Morag, R. Jelinek, *J. Colloid Interface Sci.* **2016**, *482*, 267.
[2] *Flexible Flat Panel Displays* (Ed: G. P. Crawford), John Wiley & Sons Ltd., Chichester, West Sussex, England, **2005**.
[3] Y. S. Rim, S.-H. Bae, H. Chen, N. De Marco, Y. Yang, *Adv. Mater.* **2016**, *28*, 4415.
[4] D. S. Hecht, L. Hu, G. Irvin, *Adv. Mater.* **2011**, *23*, 1482.
[5] A. Kamyshny, S. Magdassi, *Small* **2014**, *10*, 3515.
[6] J. Liang, K. Tong, Q. Pei, *Adv. Mater.* **2016**, *28*, 5986.
[7] G. Grau, J. Cen, H. Kang, R. Kitsomboonloha, W. J. Scheideler, V. Subramanian, *Flexible Printed Electron.* **2016**, *1*, 23002.
[8] T. H. J. Van Osch, J. Perelaer, A. W. M. De Laat, U. S. Schubert, *Adv. Mater.* **2008**, *20*, 343.
[9] S. Hong, J. Yeo, G. Kim, D. Kim, H. Lee, J. Kwon, H. Lee, P. Lee, S. H. Ko, *ACS Nano* **2013**, *7*, 5024.
[10] D. Lee, D. Paeng, H. K. Park, C. P. Grigoropoulos, *ACS Nano* **2014**, *8*, 9807.
[11] J. H. Park, D. Y. Lee, W. Seung, Q. Sun, S.-W. Kim, J. H. Cho, *J. Phys. Chem. C* **2015**, *119*, 7802.
[12] K. Higashitani, C. E. McNamee, M. Nakayama, *Langmuir* **2011**, *27*, 2080.
[13] M. Layani, S. Magdassi, *J. Mater. Chem.* **2011**, *21*, 15378.
[14] B. Reiser, L. Gonzalez-Garcia, I. Kanelidis, J. H. M. Maurer, T. Kraus, *Chem. Sci.* **2016**, *7*, 4190.
[15] S. Wünscher, R. Abbel, J. Perelaer, U. S. Schubert, *J. Mater. Chem. C* **2014**, *2*, 10232.

[16] M. Layani, A. Kamyshny, S. Magdassi, *Nanoscale* **2014**, *6*, 5581.
[17] K. Zilberberg, T. Riedl, *J. Mater. Chem. A* **2016**, *4*, 14481.
[18] K. Neyts, A. Real, M. Marescaux, S. Mladenovski, J. Beeckman, *J. Appl. Phys.* **2008**, *103*, 93113.
[19] P. B. Catrysse, S. Fan, *Nano Lett.* **2010**, *10*, 2944.
[20] J. H. M. Maurer, L. Gonzalez-Garcia, B. Reiser, I. Kanelidis, T. Kraus, *Nano Lett.* **2016**, *16*, 2921.
[21] B. Reiser, D. Gerstner, L. Gonzalez-Garcia, J. H. M. Maurer, I. Kanelidis, T. Kraus, *Phys. Chem. Chem. Phys.* **2016**, *18*, 27165.
[22] C.-C. Liang, M.-Y. Liao, W.-Y. Chen, T.-C. Cheng, W.-H. Chang, C.-H. Lin, *Opt. Express* **2011**, *19*, 4768.
[23] S. H. Ahn, L. J. Guo, *Adv. Mater.* **2008**, *20*, 2044.
[24] H. Feng, Y. Yang, Y. You, G. Li, J. Guo, T. Yu, Z. Shen, T. Wu, B. Xing, *Chem. Commun.* **2009**, 1984.
[25] A. Loubat, M. Impéror-Clerc, B. Pansu, F. Meneau, B. Raquet, G. Viau, L.-M. Lacroix, *Langmuir* **2014**, *30*, 4005.
[26] S. Gong, Y. Zhao, L. W. Yap, Q. Shi, Y. Wang, J. A. P. B. Bay, D. T. H. Lai, H. Uddin, W. Cheng, *Adv. Electron. Mater.* **2016**, *2*, 1600121.
[27] A. Timmann, M. Konrad, C. Schellbach, A. Meyer, D.-Hamburg, *J. Phys. Chem. B* **2005**, *109*, 1347.
[28] B. Lee, I. Park, J. Yoon, S. Park, J. Kim, K. W. Kim, T. Chang, M. Ree, *Macromolecules* **2005**, *38*, 4311.
[29] J. H. M. Maurer, L. González-García, B. Reiser, I. Kanelidis, T. Kraus, *ACS Appl. Mater. Interfaces* **2015**, *7*, 7838.
[30] J. H. M. Maurer, L. Gonzalez-Garcia, B. Reiser, I. Kanelidis, T. Kraus, *Phys. Status Solidi* **2016**, *213*, 2336.
[31] J. Van De Groep, P. Spinelli, A. Polman, *Nano Lett.* **2012**, *12*, 3138.

